Available online at www.sciencedirect.com
SCIENCE DIRECT®
Journal of Magnetic Resonance 171 (2004) 97–106
JMR Journal of Magnetic Resonance
www.elsevier.com/locate/jmr

An algorithm to calculate the NMR signal of a multi spin-echo sequence with relaxation and spin-diffusion

Yuval Zur*

TopSpin Medical (Israel) Ltd. Global Park, 2 Yodfat Street, North Industrial Zone, Lod 71291, Israel

Received 1 March 2004; revised 30 July 2004
Available online 9 September 2004

Abstract

An algorithm to calculate NMR signals of a multi-echo pulse sequence with arbitrary position dependent B_0 and B_1 fields taking into account relaxation and spin-diffusion is presented. The multi-echo pulse sequence consists of an initial RF pulse ("90°" RF pulse) and a series of L refocusing RF pulses with arbitrary phases and flip-angles. The calculation is exact and takes into account all the magnetization pathways that contribute to the signal on a predefined spatial grid. The theoretical prediction is verified experimentally using a high field NMR microscopy system. The algorithm was implemented in a simulation program in order to optimize the design of an inside-out MR intra-vascular catheter that is used for characterization of vessel wall tissue. Measured data obtained with the catheter are in good agreement with the theoretical prediction of the simulation.

Keywords: Spin-diffusion; Multi-echo sequence; Magnetization pathways; Intra-vascular catheter

1. Introduction

In this paper we present an algorithm to calculate the magnetization M and signal s of a multi-echo pulse sequence vs. time on a grid of spatial points $r = \{x_i, y_i, z_i\}$. M and s are calculated for a known position dependent static magnetic field $B_0(r)$ and RF field $B_1(r)$ by solving the Bloch Equations taking into account relaxation and spin-diffusion. The algorithm is utilized to optimize the design of a new MR intra-vascular catheter that is used for tissue characterization at the vessel wall.

Based on reference [18] we assume throughout the paper that any RF pulse can be considered an instantaneous operator applied at the RF pulse center and the evolution of the magnetization is calculated by applying free rotation, relaxation and spin-diffusion between adjacent RF pulse centers. The evolution of the magnetization along the train is analyzed using phase diagrams.

During the past few years, new NMR applications that operate in inhomogeneous fields where B_1 and B_0 vary by more than an order of magnitude over the volume of interest were developed. These applications include stray field NMR [1], oil well logging [2,3], material testing [4,5], and other applications [6] where the magnetic fields are generated from outside the sensitive volume. Such MR systems are referred to as inside-out systems [5]. The algorithm presented in this work is suitable for systems with very inhomogeneous magnetic fields such as inside-out systems and also for conventional MRI scanners.

Kiselev [7] calculated the evolution of M in a sequence with many RF pulses taking into account spin-diffusion and relaxation. In this paper we use a different although equivalent approach (see Discussion and conclusion) to solve for M and s by writing it as a finite sum of coherence pathways [8].

* Fax: +972 8 9281233.
E-mail address: zursy@netvision.net.il.

1090-7807/$ - see front matter
doi:10.1016/j.jmr.2004.07.018

An elegant analysis of the NMR signal with and without spin-diffusion using coherence pathways for a train of RF pulses with a constant inter pulse delay was given by Kaiser et al. [8]. They showed that in the presence of spin-diffusion the decay rate due to diffusion varies for different pathways. Since the number of pathways increases with the number of RF pulses an analytical calculation of the echo signal in terms of coherence pathways is not feasible. Zur et al. [9] extended this analysis to time-varying gradients with an arbitrary waveform in a steady-state free precession (SSFP) pulse sequence. Hennig [10,11] and Zur et al. [12] used phase diagrams to calculate signals in a multi-echo pulse sequence using the pioneering work of Woessner [13]. Other investigators [14–17] analyzed the signal of a multi-echo sequence based on coherence pathways and the effect of spin-diffusion on these pathways.

In the first part of the paper we shall calculate the magnetization and the signal on the grid r where $B_1(r)$, $B_0(r)$, the diffusion coefficient $D(r)$ and the relaxation times depend on r. Then we shall present an experimental verification of the algorithm using a high field MR microscopy system and an inside-out intra-vascular MR catheter.

2. Theory

A multi spin-echo pulse sequence is shown in Fig. 1. It consists of a train of L refocusing RF pulses with flip angles θ_j and phases $\varphi_j (j = 1 \text{ to } L)$, preceded by an initial RF pulse of flip angle θ_0 and phase φ_0. The j refocusing RF pulse operator is denoted P_j, and the initial RF pulse operator is denoted P_0. The time between P_0 and P_1 is τ, and between adjacent refocusing RF pulses 2τ. The center of P_0 is defined as time $t = 0$, and the center of P_j is at $t = (2j - 1)\cdot\tau$. There are L echoes and echo j is centered at $t = 2j\tau$. P_0 converts the initial longitudinal magnetization M_0 into transverse magnetization M_{xy} and subsequent refocusing RF pulses P_j refocus M_{xy} and

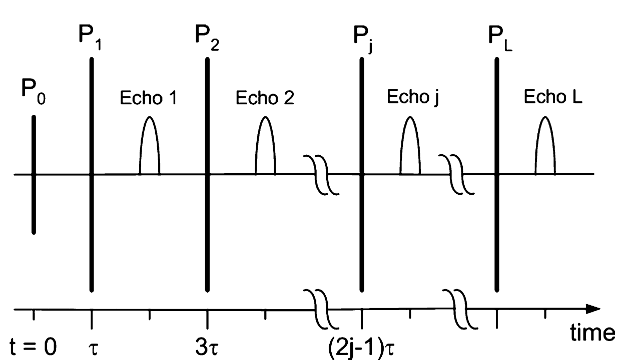

Fig. 1. A multi spin-echo pulse sequence with L refocusing RF pulses P_1 to P_L and an initial RF pulse P_0. P_0 is applied at $t = 0$ and the j RF pulse P_j at $t = (2j - 1)\cdot\tau$. The peak of echo j is at $t = 2j\tau$.

generate echoes. Hence the RF angles θ_0 and θ_j of P_0 and P_j should be close to 90° and 180°, respectively.

In many inside-out scenarios this is not possible because B_1 varies spatially. To obtain an optimal signal that is insensitive to RF imperfections we use the CPMG condition [19] that requires a phase difference of 90° between φ_0 (the phase of P_0) and φ_j (the phase of all P_j). We usually use $\varphi_0 = 0°$ and $\varphi_j = 90°$. However, M can be calculated for any arbitrary θ_j and φ_j.

The evolution of the magnetization depends on the frequency-offset $\Delta f(r)$ between the Larmor frequency of the spins and the frequency of the RF pulses, the RF field strength and the waveforms of the RF pulses. The RF field $B_1(r)$ is

$$B_1(r) = b_1(r) \cdot I(t) \cdot \cos(2\pi f_T t + \varphi), \tag{1}$$

where f_T is the frequency of the RF pulse, $b_1(r)$ is the RF field per unit current, φ is the phase of the RF pulse and $I(t)$ is a shaped current waveform designed to excite a selective volume [20]. The component of $b_1(r)$ that is perpendicular to $B_0(r)$ affects the magnetization. We denote it $b_{1p}(r)$. Since b_{1p} depends on r, the current I must be optimized for maximum signal over the excited volume.

Another consideration is the frequency dependence of the current I in the coil. The bandwidth B of the RF coil is $B = \frac{f_T}{Q}$, where f_T is the frequency of the RF pulse and Q is the quality factor of the coil. The current in the coil is very low at frequencies beyond B. For inside-out MR systems the range of Larmor frequencies usually far exceeds the coil bandwidth. Therefore current waveform $I(t)$ must be frequency selective with bandwidth smaller or equal to B while exciting a partial volume or slice. Shifting the excitation frequency f_T excites other slices until the entire volume is covered.

To calculate the evolution of the magnetization along the echo train we shall derive the RF pulse operator and the free rotation operator between RF pulses and concatenate them.

All the computations of the magnetization are done in a reference frame where B_0 is along the z-axis and b_{1p}, the perpendicular component of B_1, is in the x–y plane. This reference frame is referred to as the B_0 *frame*, and the reference frame where B_0 and B_1 are measured or simulated is referred to as the *lab frame*. b_{1p} and B_{1p} in the B_0 frame are denoted b_{1xy} and B_{1xy}, respectively, since they are in the x–y plane. The rotation operator from the lab frame to the B_0 frame is calculated on a pixel-by-pixel basis since B_0 and B_1 depend on r. The transverse and longitudinal magnetization M_{xy} and M_z are always defined and calculated in the B_0 frame.

B_{1xy} per unit current, denoted b_{1xy}, has only two components b_x and b_y. Therefore, it can be written as a complex quantity

$$b_{1xy} = b_x + ib_y, \tag{2}$$

where $i = \sqrt{-1}$. The magnetization M is written as a column vector $M = [M_{xy}, M_{xy}^*, M_z]^T$ where

$$M_{xy} = M_x + iM_y \tag{3}$$

and M_{xy}^* is the complex conjugate of M_{xy} [20].

2.1. RF pulse operator

In this section we shall write M in units of M_0, the thermal equilibrium magnetization, so that by definition $M_0 \equiv 1$. The RF pulse operator with arbitrary waveform is calculated by dividing the waveform into N piece-wise constant segments. The operator in each segment is a rotation about the effective field B_{eff}, whose magnitude and angle Θ with the z-axis are $|B_{\text{eff}}| = \sqrt{B_{1xy}^2 + \Delta B^2}$ and $\Theta = \tan^{-1}(B_{1xy}/\Delta B)$, respectively, where $\Delta B = \Delta f/\gamma$ and γ is the gyromagnetic ratio. These N rotation matrices are multiplied, yielding the RF pulse operator P. As shown in [20] the calculation of P is most efficient using the Cayley–Klein parameters $\alpha(\Delta f, B_{1xy})$ and $\beta(\Delta f, B_{1xy})$ that depend on Δf and B_{1xy}. The computation of α and β must be efficient, because they are calculated for each point on the grid.

The RF pulse operator P that operates on the column vector M is a 3-by-3 matrix given by [20]:

$$\begin{pmatrix} M_{xy}^+ \\ M_{xy}^{+*} \\ M_z^+ \end{pmatrix} = \begin{pmatrix} (\alpha^*)^2 & -\beta^2 & 2\alpha^*\beta \\ -(\beta^*)^2 & \alpha^2 & 2\alpha\beta^* \\ -\alpha^*\beta^* & -\alpha\beta & \alpha^*\alpha - \beta^*\beta \end{pmatrix} \begin{pmatrix} M_{xy}^- \\ M_{xy}^{-*} \\ M_z^- \end{pmatrix}, \tag{4}$$

where M^- and M^+ denote the magnetization before and after the RF pulse. As mentioned before, any refocusing RF pulse is equivalent to an instantaneous operator applied at the RF pulse center with free rotation and relaxation between RF pulse centers. The free rotation angle Φ during τ for a spin with Larmor frequency f_L is $\Phi = 2\pi \cdot f_L \cdot \tau$. Since M is periodic in Φ modulo 2π and all RF pulses occur at a time that is an integer multiple of τ, the magnetization $M_{xy}(\Phi)$ and $M_z(\Phi)$ immediately before and after any RF pulse j in the train is a discrete and finite sum of $\exp(im\Phi)$:

$$M_{xy}(j) = \sum_m a_m(j) \cdot \exp(im\Phi), \tag{5a}$$

$$M_z(j) = \sum_m c_m(j) \cdot \exp(im\Phi), \tag{5b}$$

where m is an integer, and $a_m(j)$, and $c_m(j)$ are independent of Φ [21]. M_z must be real for any m and Φ, therefore c_m in (5b) must be the complex conjugate of c_{-m}:

$$c_m(j) = c_{-m}^*(j). \tag{6}$$

To simplify the notation we shall remove from now on the RF pulse index j.

Eqs. (5a) and (5b) states that a finite number of coefficients a_m and c_m is required to compute M for any arbitrary Φ. This simplifies considerably the calculation of M along the echo train. Using (4) we can express the linear relation between the coefficients a_m^-, c_m^- before the RF pulse and the coefficients a_m^+, c_m^+ after it:

$$\begin{pmatrix} a_m^+ \\ a_{-m}^{+*} \\ c_m^+ \end{pmatrix} = \begin{pmatrix} (\alpha^*)^2 & -\beta^2 & 2\alpha^*\beta \\ -(\beta^*)^2 & \alpha^2 & 2\alpha\beta^* \\ -\alpha^*\beta^* & -\alpha\beta & \alpha^*\alpha - \beta^*\beta \end{pmatrix} \begin{pmatrix} a_m^- \\ a_{-m}^{-*} \\ c_m^- \end{pmatrix}, \tag{7}$$

where * denotes complex conjugate. If a_m^- and c_m^- prior to the RF pulse are known for all m, a_m^+ and c_m^+ after the RF pulse are calculated for all m using Eq. (7).

2.2. Free rotation

As shown in Appendix A, the effect of spin-diffusion during free rotation is to attenuate a_m and c_m at a rate that depends on m. Therefore, the free evolution of M_{xy} and M_z t seconds after the RF pulse is given by:

$$M_{xy}(t) = e_2 \cdot \exp(i\Omega t) \cdot \sum_m a_m(t) \cdot \exp(im\Phi), \tag{8a}$$

$$M_z(t) = e_1 \cdot \sum_m c_m(t) \cdot \exp(im\Phi) + 1 - e_1, \tag{8b}$$

where $a_m(t)$ and $c_m(t)$ are given by Eqs. (A.8) and (A.9); Ω is the Larmor angular frequency $\Omega = 2\pi f_L$; $\Phi = \Omega\tau$ is the rotation angle during τ; $e_1 = \exp(-t/T_1)$ and $e_2 = \exp(-t/T_2)$. To calculate the decay of $a_m(t)$ and $c_m(t)$ vs. t we compute the local field gradient $G \equiv \nabla|B_0(r)|$ for each voxel on the spatial grid r as explained in Appendix A.

2.3. Time evolution of $M(t)$ using phase diagrams

Phase diagrams [11,12] describe graphically the evolution of the phase of a_m and c_m vs. time along the echo train. A phase diagram for the first two refocusing RF pulses P_1 and P_2 is shown in Fig. 2. The first RF pulse P_0 converts the thermal equilibrium magnetization M_0 into transverse and longitudinal components $M_{xy}(0)$ and $M_z(0)$, respectively. Since $M_{xy}(0)$ and $M_z(0)$ are independent of Φ the expansion in (5a) and (5b) consists of only one coefficient with $m = 0$, i.e., $M_{xy}(0) = a_0$ and $M_z(0) = c_0$. During τ a_0 and c_0 evolve according to (8a) and (8b): a_0 decay due to T_2 and diffusion while acquiring a phase Φ, and c_0 undergoes T_1 relaxation and attenuation due to diffusion. Prior to P_1 there is one transverse component a_1^- with phase Φ that originate from a_0 and one longitudinal component c_0^-:

$$a_1^- = E_2 \cdot \exp(i\Phi) \cdot a_0(\tau), \tag{9a}$$

$$c_0^- = E_1 \cdot c_0 + 1 - E_1, \tag{9b}$$

where $\Phi = \Omega\tau$, $E_1 = \exp(-\tau/T_1)$ and $E_2 = \exp(-\tau/T_2)$. $a_0(\tau)$ is obtained by substituting $m = 0$ and $t = \tau$ in

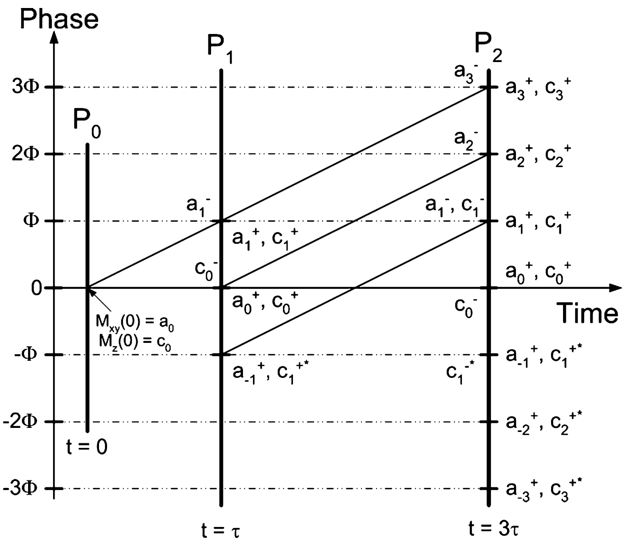

Fig. 2. Phase diagram of the first two RF pulses P_1 and P_2. Φ is the free rotation angle during τ. The magnetization immediately after RF pulse j is a discrete sum of $4j-1$ complex exponents with coefficients a_m and c_m and phase $m\Phi$ where $m = -(2j-1)$ to $2j-1$.

(A.8). According to (7) P_1 splits a_1^- into a_1^+ and a_{-1}^+ with phase Φ and $-\Phi$, respectively and into c_1^+ and c_1^{+*} with phase Φ and $-\Phi$. c_0^- is split into a_0^+ and c_0^+. During the time 2τ between P_1 and P_2, a_{-1}^+, a_0^+, and a_1^+ decay due to T_2 and diffusion and acquire a phase of 2Φ radians. Similarly c_1^+, c_0^+, and c_1^{+*} undergo T_1 relaxation and diffusion. Prior to P_2 there are three transverse components a_m^- with $m = 1, 2$, and 3 and phases Φ, 2Φ, and 3Φ, and 3 longitudinal components c_m^- with $m = -1, 0, 1$, and phases $-\Phi, 0, \Phi$. P_2 converts them into 7 transverse and longitudinal components a_m^+ and c_m^+ with $m = -3$ to 3 and phases -3Φ to 3Φ. In general, after RF pulse j there are $4j-1$ transverse components a_m^+ and $4j-1$ longitudinal components c_m^+ with m going from $-(2j-1)$ to $2j-1$. Therefore, the sum over m in (5a), (5b), (8a), and(8b) is finite with $|m| \leqslant 2j-1$. In Eq. (7) $m = 0$ to $2j-1$ since a_m and a_{-m} are calculated simultaneously.

Finally a_m^+ and c_m^+ are calculated for all the RF pulses in the train by going from the first to the last RF pulse using (7), (8a), and (8b). These calculations are carried out for all relevant spatial locations, because a_m^+ and c_m^+ depend on r through α and β.

2.4. Calculation of echo magnetization

So far we have calculated $M(t)$ at a given spatial position r. To compute the magnetization for the whole sample we integrate $M(t)$ in Eqs. (8a) and (8b) over r.

$$m_{xy}(t) = \int_r M_0(r) \cdot e_2 \cdot \exp[\mathrm{i}\Omega(r) \cdot t] \sum_m a_m(r,t) \cdot \exp[\mathrm{i}m\Phi(r)] \cdot \mathrm{d}r, \tag{10}$$

where $M_0(r)$ is the local equilibrium magnetization, which is proportional to the local field $B_0(r)$ and $\Phi(r) = \Omega(r)\cdot\tau$ is the phase acquired during τ. $m_{xy}(t)$ may be written as a sum over m of echo magnetizations where echo m is given by

$$m_{xy}^{\mathrm{echo}}(m,t) = \int_r M_0(r) \cdot e_2 \cdot a_m(t,r) \cdot \exp\{\mathrm{i}[\Omega(r) \cdot t + m\Omega(r) \cdot \tau]\} \cdot \mathrm{d}r. \tag{11}$$

The detected signal $s(t)$ is proportional to $m_{xy}(t)$ [22] and is sampled over a finite time window $W(t)$, which is usually a square window of T seconds. Therefore the sampled magnetization $\tilde{m}_{xy}(t)$ is a multiplication of $m_{xy}(t)$ and $W(t)$.

$$\tilde{m}_{xy}(t) = m_{xy}(t) \cdot W(t) \tag{12}$$

$m_{xy}(t)$ reaches a peak at a time $t = t_{\mathrm{echo}}$ when the phase $\Omega(r)\cdot t_{\mathrm{echo}} + m\Omega(r)\cdot\tau$ of echo m in (11) is zero, so that $t_{\mathrm{echo}} = -m\cdot\tau$. Since $0 \leqslant t \leqslant 2\tau$ there are three echoes at $t_{\mathrm{echo}} = 0, \tau$, and 2τ. If the time difference between these echo peaks is equal or greater than the sampling window duration, the window $W(t)$ can be located close to any single echo peak and the sampled magnetization $\tilde{m}_{xy}(t)$ consists of this single echo with negligible contributions from other echoes. For our sequence the sampling window is centered at $t_{\mathrm{echo}} = \tau$ so that $\tilde{m}_{xy}(t)$ consists of a single echo with $m = -1$. From (11):

$$\tilde{m}_{xy}(t) = \int_r M_0(r) \cdot e_2 \cdot a_{-1}(r,t) \cdot \exp[\mathrm{i}\Omega(r) \cdot (t-\tau)] \cdot \mathrm{d}r. \tag{13a}$$

That can be rewritten as

$$\tilde{m}_{xy}(t) = \int_r M_{xy}^{\mathrm{echo}}(r) \cdot \exp[\mathrm{i}\Omega(r) \cdot (t-\tau)] \cdot \mathrm{d}r, \tag{13b}$$

where

$$M_{xy}^{\mathrm{echo}}(r) = M_0(r) \cdot E_2 \cdot a_{-1}(r,\tau) \tag{14}$$

$a_{-1}(r,\tau)$ at $t = \tau$ is calculated from a_{-1}^+ using (A.8). As expected, the echo magnetization $M_{xy}^{\mathrm{echo}}(r)$ at r is the Fourier transform of $\tilde{m}_{xy}(t)$.

The longitudinal magnetization of the sample is obtained by integrating Eq. (8b) over r:

$$m_z(t) = \int_r M_0(r) \cdot \left\{ e_1 \cdot \sum_m c_m(t,r) \cdot \exp[\mathrm{i}m\Phi(r)] + 1 - e_1 \right\} \cdot \mathrm{d}r. \tag{15}$$

As before, $\tilde{m}_z(t) = m_z(t) \cdot W(t)$ is found by setting the phase factor in (15) to zero so that $m = 0$:

$$\tilde{m}_z(t) = \int_r M_z^{\mathrm{echo}}(r) \cdot \mathrm{d}r = \int_r M_0(r) \cdot [e_1 \cdot c_0(r,t) + 1 - e_1] \cdot \mathrm{d}r, \tag{16}$$

where $M_z^{\text{echo}}(r)$ is the longitudinal magnetization at location r and time $t = \tau$:

$$M_z^{\text{echo}}(r) = M_0(r) \cdot [E_1 \cdot c_0(r,\tau) + 1 - E_1] \tag{17}$$

$c_0(r, \tau)$ is c_0 at $t = \tau$.

$M_z^{\text{echo}}(r)$ and $M_{xy}^{\text{echo}}(r)$ are calculated for all the RF pulses over the grid r using (14) and (17).

2.5. Strategies to minimize computation time

Minimization of computation time is very critical for systems with inhomogeneous fields because there are many RF pulses and because a dense grid of points in space is required to calculate the magnetization and the signal accurately. In this section we shall show how to minimize the number of calculations while preserving accuracy. In previous sections we have calculated a_m^+ and c_m^+ for all m. However, to compute the echo magnetization $M^{\text{echo}}(r)$ we need only a_{-1}^+ and c_0^+. Therefore, we have to calculate only those a_m and c_m that contribute to a_{-1}^+ and c_0^+ along the train.

Fig. 3 shows a phase diagram with $L = 5$ RF pulses. As we know there are $4j - 1$ coefficients with $|m| \leqslant 2j - 1$ after RF pulse j. We have drawn a subset of these values with $|m| \leqslant 1, 3, 5, 3, 1$ after P_1 to P_5, respectively. It can be seen by inspection that only coefficients with m values within the subset in Fig. 3 contribute to a_{-1}^+ and c_0^+ after *any* of the $L = 5$ RF pulses, so that m values outside this subset can be ignored. For example a_m^+ or c_m^+ with $m = 4$ immediately after P_4 will not contribute to a_{-1}^+ or c_0^+ after P_4 or P_5. This can be generalized by reducing the RF pulse number j to an *effective* RF pulse number J_{eff} such that the subset of m values that we use after RF pulse j is $N = 4J_{\text{eff}} - 1$ rather than $4j - 1$, with $|m| \leqslant 2J_{\text{eff}} - 1$. The effective RF pulse number J_{eff} for RF pulse j is given by:

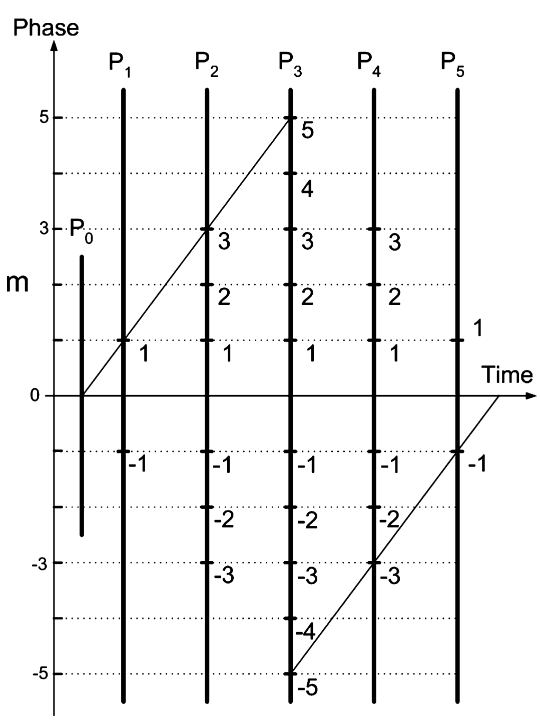

Fig. 3. Phase diagram of $L = 5$ refocusing RF pulses. There are 3, 7, 11, 15, and 19 a_m coefficients after P_1 to P_5, respectively, with $|m| \leqslant 1$, 3, 5, 7, and 9. The m values shown in this figure are a subset with $|m| \leqslant 1$, 3, 5, 3, and 1. Only m values within this subset contribute to a_{-1}^+ after *any* of the L RF pulses.

$$J_{\text{eff}} = j \quad \text{for } j \leqslant (L+1)/2, \tag{18a}$$

$$J_{\text{eff}} = L + 1 - j \quad \text{for } j > (L+1)/2. \tag{18b}$$

In Fig. 3 where $L = 5$ and $j = 1$–5, $J_{\text{eff}} = 1, 2, 3, 2, 1$ with $|m| \leqslant 1, 3, 5, 3, 1$, respectively. By using $|m| \leqslant (2J_{\text{eff}} - 1)$ instead of $|m| \leqslant (2j - 1)$ the number of coefficients a_m and c_m that have to be calculated decrease by a factor of 2.

In many applications we need only the echo transverse magnetization M_{xy}^{echo} in (14) and we do not have to calculate M_z^{echo}. In this case only coefficients that contribute to a_{-1}^+ should be computed. From Eq. (7) and the phase diagrams in Figs. 2 and 3 we find that an RF pulse or a free rotation operator cannot transform a_m or c_m with even m value into a_m or c_m with odd m value and vice versa. Therefore, only coefficients with odd m values contribute to a_{-1}^+ along the echo train ($m = -1$ is odd), and all the coefficients with even m values can be ignored.

In summary, the number of coefficients that have to be calculated decreases by approximately a factor of 2, from $4j - 1$ to $4J_{\text{eff}} - 1$. If we do not calculate M_z^{echo} a further reduction by another factor of 2 is possible because a_m and c_m with even m values can be ignored.

2.6. Signal amplitude calculation

The calculation of the signal and the magnetization is done in the B_0 frame, where the local $B_0(r)$ is along the z-axis. The signal $s_j(r)$ after RF pulse j is calculated on a discrete spatial grid $r = \{x_i, y_i, z_i\}$. $s_j(r)$ is given by [22]:

$$s_j(r) = \Omega(r) \cdot \mathrm{d}V \cdot |\boldsymbol{b}_{1xy}| \cdot |M_{xy}^{\text{echo}}(r)| \cdot \exp(\mathrm{i}\beta), \tag{19}$$

where $|\boldsymbol{b}_{1xy}|$ and $|M_{xy}^{\text{echo}}(r)|$ are the modulus of the complex numbers $\boldsymbol{b}_{1xy}$ Eq. (2) and $M_{xy}^{\text{echo}}(r)$ Eq. (14), respectively, and β is the angle between them; $\Omega(r)$ is the angular Larmor frequency of the spin at r and $\mathrm{d}V$ is the volume of the voxel on the grid at r. When the same RF coil is used for excitation and detection β is constant for all r. $M_{xy}^{\text{echo}}(r)$ precesses at an angular Larmor frequency Ω, so that the signal vs. time is $s_j(r) \cdot \exp(\mathrm{i}\Omega(r) \cdot t)$. The detected signal $S_j(t)$ from the excited volume after RF pulse j is a sum of the signals from all the voxels:

$$S_j(t) = \sum_{\text{voxels}} s_j(r) \cdot \exp(\mathrm{i}\Omega(r) \cdot t). \tag{20}$$

Hence $S_j(t)$ is the discrete inverse Fourier transformation of $s_j(r)$. The signal at the peak of echo j where all the voxels are approximately in phase is

$$S_j = \sum_{\text{voxels}} s_j(r). \tag{21}$$

We have to calculate $s_j(r)$ for all the points on the grid for all the echoes. This is a very demanding task when the number of RF pulses and/or the number of points on the spatial grid is large. For spatially inhomogeneous fields the grid must be dense enough to assure good accuracy and the time between adjacent RF pulses must be short (i.e., a few microseconds) to prevent fast signal decay due to diffusion. In typical cases the total number of points on the grid exceeds 10^5 with over 1000 RF pulses. To reduce the computational load we calculate $s_j(r)$ for only the first 50–100 RF pulses and fit the time decay of each voxel to a mono-exponential function with time constant $T_c(r)$ while ignoring the first 3–5 echoes. The approximation of $s_j(r)$ along the echo train to a mono-exponential function reduces computation time significantly while preserving accuracy. The signal S_j at the peak of echo j Eq. (21) at time $t_j = 2j\tau$ is given by

$$S_j = \sum_{\text{voxels}} s_1(r) \cdot \exp[-t_j/T_c(r)], \tag{22}$$

where $s_1(r)$ is the signal of the first echo we use. This is very economical in computer resources, because only $s_1(r)$ and $T_c(r)$ needs to be computed and stored in memory for each voxel instead of the vector $s_j(r)$ for all j. Since S_j decays with time along the echo train due to T_1, T_2 and spin-diffusion, it can be fitted to an exponential function and this fit yields the time constant τ_c:

$$S_j = S_1 \cdot \exp(-t_j/\tau_c), \tag{23}$$

where S_1 is the signal of the first echo that we use and $t_j = 2j\tau$ is the echo time along the train. We have found that the approximation of S_j to a single exponential decay in (23) is excellent with no visible difference between the two. In the experimental section below we shall compare the calculated and measured time constant τ_c of S_j from an inside-out MR catheter.

2.7. Algorithm implementation

A simulation program was written in MATLAB (MathWorks, Natick Mass. USA) to calculate the echo magnetization and the signal along the echo train on an arbitrary 3D spatial grid r with known $B_0(r)$ and $B_1(r)$. The program calculates the RF waveform and optimal current taking into account the known impulse response of the RF coil. The gradient $G \equiv \nabla|B_0(r)|$ is computed for all the voxels in r as explained in Appendix A. The echo magnetization and signal from each voxel Eq. (19) and from the whole excited volume Eq. (22) are calculated along the echo train. The relaxation times and the diffusion constant D are defined on a pixel-by-pixel basis. This enables us to test tissue contrast and any other desired parameter for structures with arbitrary morphology.

To demonstrate the performance of the simulation we computed the echo magnetization of a CPMG pulse train with $L = 50$ selective refocusing RF pulses (3 kHz bandwidth and 3 ms duration) with an RF flip angle of 180° in a uniform B_1 field and a B_0 with a constant gradient $G = 10$ Gauss/cm. Sample parameters are $T_1 = 2000$ ms, $T_2 = 1000$ ms, and $D = 2.0 \times 10^{-9}$ m²/s. The time between echoes is $2\tau = 10$ ms. Figs. 4A and B show a 2D plot of the y-component of M_{xy}^{echo} and M_z^{echo}, respectively, for $j = 1$–50 RF pulses vs. r with a grid of 50 equally spaced points from -1.17 to 1.17 mm. The negative value of M_z is displayed in Fig. 4B to better visualize the data. The selective RF pulse excites a 0.7 mm slice centered at $r = 0$, and M_{xy}^{echo} decays with a time constant of 74 ms. This calculation was

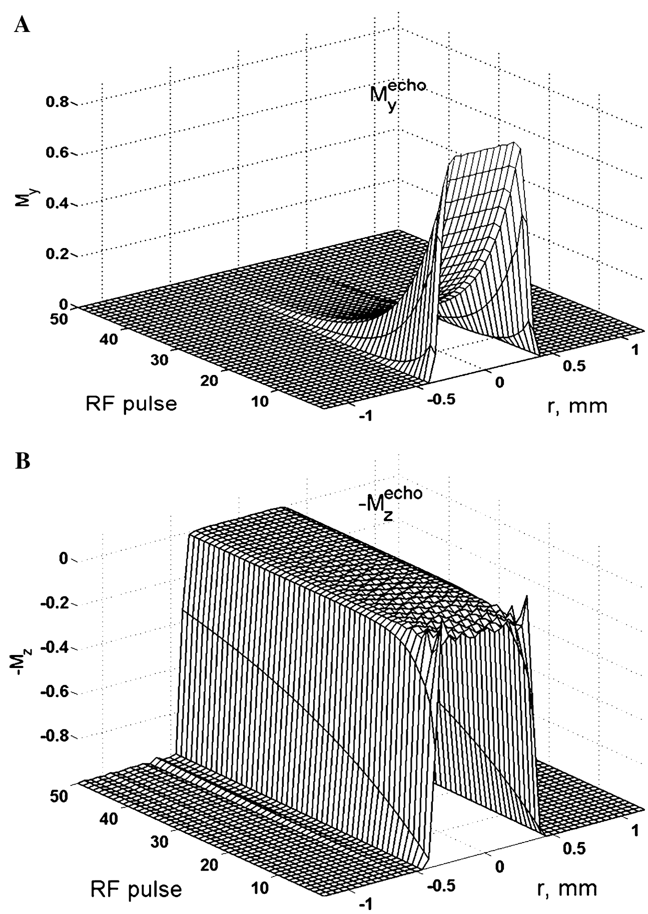

Fig. 4. The y component of M_{xy}^{echo} (A) and $-M_z^{\text{echo}}$ (B) along a CPMG pulse train with $L = 50$ selective refocusing RF pulses vs. spatial position r. The negative value of M_z is displayed in (B) to better visualize the data. The spatial grid consists of 50 equally spaced points from -1.17 to 1.17 mm with a field gradient of $G = 10$ Gauss/cm with $2\tau = 10$ ms between echoes.

completed in about 0.4 s using MATLAB 6.1 on a 700 MHz PC computer. The computation time decreased to 0.1 s when we used the above-mentioned strategies to reduce computation time by a factor of 4.

3. Experimental results

3.1. Measurements with a high field NMR microscopy system

To verify the theory we measured the decay time constants of water with known diffusion coefficient and relaxation times at various RF flip angles and gradient amplitudes and compared it to the decay rates calculated by the theory. The measurements were performed on a high field NMR system equipped with magnetic field gradients operating at 400 MHz (Bruker Avance 400 WB, Bruker. Karlsruhe Germany). We used a sample of doped water at 20 °C with diffusion coefficient $D = 2.0 \times 10^{-9}$ m^2/s. The RF flip angle was calibrated with a gradient echo pulse sequence and the gradient amplitude was calibrated by applying gradient pulses with a known current and measuring the shift of the resonance line.

We used a CPMG pulse sequence with 100 refocusing RF pulses, 4.1 ms between echoes and a sampling rate of 16 kHz. The RF pulses were sinc pulses with 3 lobes. Each data set was acquired in two experiments, where the phase of the 90° RF pulse was inverted in the second experiment and the results subtracted to eliminate baseline and systematic errors. The sampled data was separated into echoes and each echo was Fourier transformed and phase corrected. The measured signal of each echo was calculated by summing the relevant points within that echo. We sampled all the $L = 100$ echoes and created a vector S with 100 points acquired at the echo centers of the CPMG pulse train. The vector S was fitted to an exponential function, which gave the time constant of the decay of the measured signal. The theoretical signal vector S was calculated in a similar way by running the simulation program with the same sinc RF pulses and summing the points within each echo. The time constant of the decay of the calculated signal was obtained by a least squares exponential fit.

The longitudinal relaxation time T_1 of the water sample, measured with an inversion recovery pulse sequence, was 910 ms. T_2 was measured by running the CPMG pulse sequence at zero gradient and RF flip angle of 180° (experiment number 10 in Table 1). The measured time constant of 216 ms depends slightly on T_1 through stimulated echo pathways. To determine T_2 accurately we calculated the time constant of the signal (using our program) with zero gradient as a function of T_2 for $T_1 = 910$ ms. We found that a time constant of 216 ms corresponds to $T_2 = 200$ ms. These T_1 and T_2 values were used in the calculation of the theoretical time constants.

The measured and calculated time constants for various RF flip angles and gradient amplitudes are listed in Table 1. The agreement between calculated and measured values is good in all cases.

3.2. Results from an inside-out NMR intra-vascular catheter

In this section we present calculated and measured data obtained with an MR intra-vascular catheter developed by TopSpin Medical (Lod, Israel). The purpose is to demonstrate the agreement between measured and calculated data. A detailed description of the catheter is presented elsewhere [23].

The catheter, shown schematically in Fig. 5, is an inside-out system with a pair of miniature Nd Fe permanent magnets (Vac, Hanau, Germany) of 1.6 mm diameter and 3 mm length for each magnet, separated by an air gap of 0.9 mm. A miniature solenoid transmit/receive RF coil of 2 mm length by 1 mm width by 0.2 mm height with 110 turns centered at the air gap between the magnets generates the RF field $B_1(r)$. The magnets are magnetized at an angle of 45° with respect to the magnet axis (the z-axis) as depicted in Fig. 5 in order to maximize B_0 at the sensitive region of the RF coil. Close to the center of the coil at $z = 0$ the B_0 field lines are

Table 1
Measured and calculated time constants along a CPMG echo train of a sample of doped water vs. gradient strength and RF flip angle

Experiment	RF flip angle (°)	Gradient (Gauss/cm)	Measured TC (ms)	Calculated TC (ms)
1	180	40	25.3	25.9
2	180	20	74.7	75.3
3	180	10	151	144.4
4	90	40	19.3	18.4
5	90	20	62.3	60.6
6	90	10	145	142.8
7	45	40	12.7	12.9
8	45	20	46.8	46.6
9	45	10	125	130
10	180	0	216	

Sample parameters: $D = 2.0 \times 10^{-9}$ m^2/s, $T_1 = 910$ ms, $T_2 = 200$ ms. The data were acquired with a 400 MHz MR microscopy system.

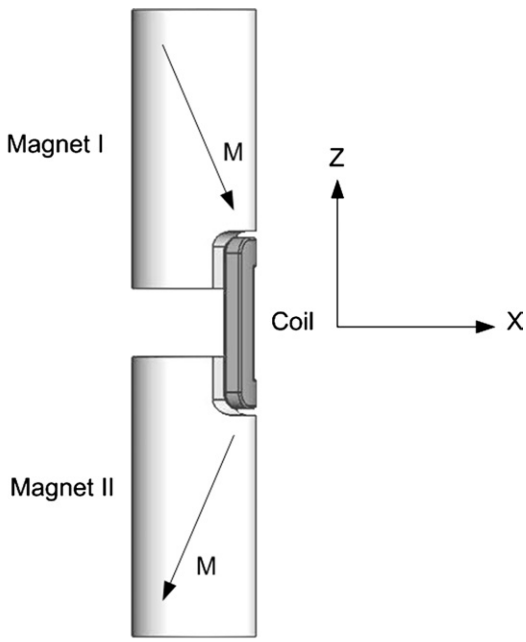

Fig. 5. The MR catheter for intra-vascular tissue characterization. The catheter consists of two permanent Nd Fe magnets of 1.6 mm diameter and 3 mm length separated by a 0.9 mm air gap and a 2 mm × 1 mm by 0.2 mm solenoid RF coil. The magnets are magnetized at an angle of 45° with respect to the z-axis in order to maximize B_0 at the sensitive volume near the RF coil. Close to the center of the RF coil B_0 is along the z-axis and B_1 is along the x-axis.

approximately parallel to the z-axis and the B_1 field lines are parallel to the x-axis. During data acquisition the catheter is attached mechanically to the vessel wall for tissue characterization.

To calculate the signals from the catheter the fields $B_0(r)$ and $B_1(r)$ were measured with a Hall probe with a resolution of 50 μm and interpolated to a resolution of 20 μm for $x = 0.8$–1.5 mm, $y = -1$ to 1 mm, and $z = -1.5$ to 1.5 mm. A CPMG pulse sequence with 3000 RF pulses of 2 μs duration and 1 MHz bandwidth with $2\tau = 11.6\,\mu s$ between RF pulse centers was applied on a doped water sample ($D = 2 \times 10^{-9}$ m²/s, $T_1 = 200$ ms, and $T_2 = 100$ ms). The bandwidth of the RF pulses was calculated from the impulse response of the RF coil with $Q \approx 12$. Two volumes, centered at a distance of about 50 and 150 μm from the coil where B_0 is 0.23 and 0.2 T, respectively, were excited by setting the frequency of the RF pulses to 9.5 MHz and then to 8.5 MHz. The field gradient $G(r) \equiv \nabla|B_0(r)|$ was calculated from the measured field for all the voxels in the excited volumes. The *average* gradient for the volumes at 9.5 and 8.5 MHz was 370 and 320 T/m, respectively. The signal $s_1(r)$ and the time constant $T_c(r)$ were computed for all the relevant voxels using $G(r)$, D, T_1, and T_2. The signal S_j at the peak of echo j was calculated for all the echoes j = 1–3000 using Eq. (21). Finally the time constant τ_c (Eq. (23)) for both volumes was obtained by fitting S_j to an exponential function.

Table 2
Measured and calculated time constants τ_c (Eq. (23)) along a CPMG echo train of a water sample using the intra-vascular MR catheter shown in Fig. 5

RF frequency (MHz)	Measured τ_c (ms)	Calculated τ_c (ms)
9.5	2.8 ± 0.24	2.77
8.5	3.2 ± 0.4	3.50

Sample parameters: $D = 2.0 \times 10^{-9}$ m²/s, $T_1 = 200$ ms, $T_2 = 100$ ms. The errors of the measured τ_c are derived from the standard deviation of the noise.

To verify the results of the simulation experimentally, the decay of the echo signal along the train was measured with the MR catheter. During the experiment the catheter was immersed in the doped water sample, and echoes from the above-mentioned CPMG sequence were acquired from the two volumes at 8.5 and 9.5 MHz with a repetition time (TR) of 200 ms with 200 signal averages. The measured time constant τ_c was derived by fitting the signal at the peak of the echoes along the train to an exponential function. The calculated and measured time constants for both volumes are listed in Table 2. The deviation between measured and calculated time constants at both frequencies is within the root mean square (rms) error caused by the standard deviation of the noise in the measured data. The error at 8.5 MHz is higher because the signal-to-noise ratio is lower due to its larger distance from the coil center.

4. Discussion and conclusion

The algorithm presented in this work computes the time evolution of the magnetization M and signal s on a predefined spatial grid taking into account relaxation and spin-diffusion.

The accuracy and efficiency of the calculation stems from the fact that M_{xy} after RF pulse j is a polynomial of exp(iΦ) with $N = 4j - 1$ coefficients a_m Eqs. (5a) and (5b):

$$M_{xy}(\Phi) = \sum_{m=-(2j-1)}^{2j-1} a_m \cdot \exp(\mathrm{i}m\Phi). \tag{24}$$

It can be shown [24] that a_m can be derived from $M_{xy}(\Phi)$ evaluated (using Eq. (24)) at N discrete values of Φ around the unit circle, i.e., at $\Phi_k = \frac{2\pi}{N}k$ radians with $k = -(2j-1)$ to $2j-1$:

$$M_{xy}(\Phi_k) = \sum_{m=-(2j-1)}^{2j-1} a_m \cdot \exp\left(\mathrm{i}m \cdot \frac{2\pi}{N}k\right). \tag{25a}$$

From reference [24] a_m is the inverse discrete Fourier transform of $M_{xy}(\Phi_k)$:

$$a_m = \frac{1}{N} \sum_{k=-(2j-1)}^{2j-1} M_{xy}(\Phi_k) \cdot \exp\left(-\mathrm{i}m \cdot \frac{2\pi}{N}k\right). \tag{25b}$$

Similar expressions can be derived for $M_z(\Phi_k)$ and c_m. Therefore the magnetization M can be equivalently characterized either by the coefficients a_m and c_m or by $M_{xy}(\Phi_k)$ and $M_z(\Phi_k)$. Kiselev [7] uses $M_{xy}(\Phi_k)$ and $M_z(\Phi_k)$, whereas in this work we use a_m and c_m. Consequently both solutions are equivalent in terms of computation time.

The approach presented in this paper has the following advantages: (i) Based on the RF pulse operator in Eq. (7) the evolution of M can be described graphically using phase diagrams, allowing a simple way to follow the evolution of M along the train. (ii) Using phase diagrams we were able to reduce computation time by a factor of 4 as explained above. (iii) The magnetization of echo m is simply proportional to a_m (Eqs. (11) and (14)) such that the calculation of the magnetization of *any* echo is trivial.

The RF pulse dependence on off-resonance Δf is incorporated through α and β in Eq. (7). This is important for systems with inhomogeneous fields where the bandwidth of the RF pulses is narrower than the range of Larmor frequencies of the spins in the examined volume. The method can be easily extended to any other sequence by concatenating RF pulse operators (Eq. (7)) and free evolution operators (Eqs. (8a) and (8b)).

A well-known technique to create diffusion-weighted images is to prepare a diffusion weighted *initial* magnetization a_0 and c_0 (Eqs. (9a) and (9b)) before running the multi-echo sequence [25–27]. The preparation phase can be a stimulated echo or a spin-echo sequence with long gradient lobes. Our algorithm may be used to compute the signal of any diffusion weighed sequence: a_0 and c_0 are calculated using Eqs. (A.8), (A.9) or (A.5), and the signal decay along the echo train is computed as explained before. Note that when time varying gradients are employed the general expression Eq. (A.5) must be used instead of Eqs. (A.8) and (A.9) and the factor F calculated from the known gradient waveform. In some applications [25,26] it is necessary to separate the signal into even and odd echoes [12]. In this case the echo train is calculated twice employing a phase cycling scheme as explained in [12] with signals s_1 and s_2. The even (odd) echoes are calculated by adding (subtracting) s_1 and s_2.

The method presented in this work was implemented in a simulation program that computes and displays the magnetization and signals from all the voxels on a spatial grid for all the echoes along the train using measured or simulated fields $B_0(r)$ and $B_1(r)$. Measured data obtained with a high field NMR microscopy system and an intra-vascular MR catheter agree with the theoretical prediction of the simulation. This simulation program is utilized to optimize the design of the magnets and RF coil configuration of the MR catheter.

Acknowledgments

The author gratefully acknowledges Lev Muchnik for writing a major part of the simulation program code, Dr. Peter Bendel from the Weizmann Institute of Science in Rehovot, Israel for running the high field NMR system, and Assaf Weiss for running the measurements of the MR Intra-vascular catheter.

Appendix A

The free solution (without RF) of the Bloch equations with diffusion can be found in reference [9] based on references [8] and [28]. In this Appendix we generalize this solution to the case of inhomogeneous B_0 and B_1 fields.

The magnetization between RF pulse j and $j+1$ is given by (Eqs. (8a) and (8b)):

$$M_j^+(t,\Phi) = e_2 \cdot \exp(\mathrm{i}\phi) \cdot \sum_m a_m(j,t)\exp(\mathrm{i}m\Phi), \tag{A.1}$$

$$M_j^z(t,\Phi) = e_1 \cdot \sum_m c_m(j,t)\exp(\mathrm{i}m\Phi) + 1 - e_1, \tag{A.2}$$

where $t = 0$ is defined as the time immediately after RF pulse j, $0 \leqslant t < 2\tau$ and $m = -(2j-1)$ to $2j-1$. We shall calculate the evolution in time due to diffusion of $a_m(t)$ and $c_m(t)$ in (A.1) and (A.2). Φ and ϕ in (A.1) and (A.2) are the precession angle around the local static magnetic field at the Larmor frequency f_L from $t = 0$ to $t = \tau$ and from $t = 0$ to $t = t$:

$$\Phi = \int_0^\tau 2\pi \cdot f_L(t') \cdot \mathrm{d}t', \tag{A.3}$$

$$\phi(t) = \int_0^t 2\pi \cdot f_L(t') \cdot \mathrm{d}t', \tag{A.4}$$

where $f_L(t)$ is the Larmor frequency at time t:

$$f_L = \frac{-\gamma}{2\pi} \cdot |B_0(r)|$$

and $|B_0(r)|$ is the vector magnitude of B_0 at r.

The time evolution of $a_m(t)$ is given by Eqs. (7) and (8) in reference [9]:

$$a_m(t) = a_m(0) \cdot \exp\left(-D\int_0^t F(m,t')\mathrm{d}t'\right), \tag{A.5}$$

where $F(m,t) = m^2 \cdot \Phi_r^2 + 2m \cdot \Phi_r \cdot \phi_r + \phi_r^2$, where $\Phi_r \equiv \nabla\Phi$, the spatial gradient of Φ, and $\phi_r \equiv \nabla\phi$. D is the isotropic diffusion coefficient.

Usually B_0 is constant in time but vary spatially. We expand the vector *magnitude* of $B_0(r)$ in a Taylor series $|B_0(r)| \approx B_0^0 + \nabla|B_0(r)| \bullet r$, where B_0^0 is a constant, $\nabla|B_0(r)|$ is the spatial gradient of $|B_0(r)|$ and $\bullet$ is dot vector multiplication. To simplify the Equations we define $G \equiv \nabla|B_0(r)|$. For time-independent $B_0(r)$ we obtain for ϕ and Φ:

$$\Phi = 2\pi f_L \tau = -\gamma \cdot |B_0(r)|\tau = -\gamma B_0^0 \tau - \gamma\tau G \bullet r, \quad (A.6)$$

$$\Phi_r = \nabla\Phi = -\gamma\tau G,$$

$$\phi = -\gamma B_0^0 t - \gamma t G \bullet r, \quad (A.7)$$

$$\phi_r = \nabla\phi = -\gamma t G.$$

From Eqs. (A.5), (A.6), and (A.7):

$$a_m(t) = a_m(0) \cdot \exp\left\{-DG^2 \cdot [m^2\gamma^2\tau^2 t + m\gamma^2\tau \cdot t^2 + \gamma^2 \cdot t^3/3]\right\}, \quad (A.8)$$

and G^2 is the square magnitude of G.

The time evolution of $c_m(t)$ is given in Eq. (13) of reference [9]. Using (A.6) and (A.7):

$$c_m(t) = c_m(0) \cdot \exp[-DG^2 \cdot m^2\gamma^2 \cdot \tau^2 t]. \quad (A.9)$$

Note that Eqs. (A.8) and (A.9) hold only for an isotropic diffusion constant D. In case of an anisotropic diffusion D becomes a tensor with values D_{11}, D_{22}, and D_{33} along the principal axes of the tensor. The expression DG^2 in Eqs. (A.8) and (A.9) is replaced by

$$DG^2 \to D_{11} \cdot G_1^2 + D_{22} \cdot G_2^2 + D_{33} \cdot G_3^2, \quad (A.10)$$

G_1, G_2, and G_3 are the components of G along the principal axes of the tensor D.

References

[1] P.J. McDonald, Stray field magnetic resonance imaging, Prog. Nucl. Magn. Reson. Spectrosc. 30 (1997) 69–99.
[2] G.R. Coates, L. Xiao, M.G. Prammer, NMR Logging: Principles and Applications, Gulf Publishing Company, Houston, 1999.
[3] D.E. Woessner, The early days of NMR in the southwest, Concepts Magn. Reson. 13 (2001) 77–102.
[4] G. Eidmann, R. Savelsberg, P. Blumler, B. Blumich, The NMR MOUSE, a mobile universal surface explorer, J. Magn. Res. A 122 (1996) 104–109.
[5] S. Anferova, V. Anferov, M. Adams, P. Blumler, N. Routley, K. Hailu, K. Kupferschlager, M.J.D. Mallett, G. Schroeder, S. Sharma, B. Blumich, Construction of a NMR MOUSE with short dead time, Concepts Magn. Reson. 15 (1) (2002) 15–25.
[6] V.S. Grechishkin, N.Y. Sinyavskii, New technologies: nuclear quadrupole resonance as an explosive and narcotic detection technique, Phys. Uspekhi 40 (1997) 393–406.
[7] V.G. Kiselev, Calculation of diffusion effect for arbitrary pulse sequences, J. Magn. Res. 164 (2003) 205–211.
[8] R. Kaiser, E. Bartholdi, R.R. Ernst, Diffusion and field gradient effects in NMR Fourier spectroscopy, J. Chem. Phys. 60 (1974) 2966–2979.
[9] Y. Zur, E. Bosak, N. Kaplan, A new diffusion SSFP imaging technique, Mag. Res. Med. 37 (1997) 716–722.
[10] J. Hennig, Multiecho imaging sequences with low refocusing flip angles, J. Magn. Res. 78 (1988) 397–407.
[11] J. Hennig, Echoes how to generate, recognize, use or avoid them in MR imaging sequences, Concepts Magn. Reson. 3 (1991) 125–143.
[12] Y. Zur, S. Stokar, A phase cycling technique for canceling spurious echoes in NMR imaging, J. Magn. Res. 71 (1987) 212–228.
[13] D.E. Woessner, Effects of diffusion in nuclear magnetic resonance spin-echo experiments, J. Chem. Phys. 34 (1961) 2057–2061.
[14] M.D. Hurlimann, Diffusion and relaxation effects in general stray field NMR experiments, J. Magn. Res. 148 (2001) 367–378.
[15] F. Balibanu, K. Hailu, R. Eymael, D.E. Demco, B. Blumich, Nuclear magnetic resonance in inhomogeneous magnetic fields, J. Magn. Res. 145 (2000) 246–258.
[16] Y.Q. Song, Categories of coherence pathways for the CPMG sequence, J. Magn. Res. 157 (2002) 82–91.
[17] M.D. Hurlimann, Carr–Purcell sequences with composite pulses, J. Magn. Res. 152 (2001) 109–123.
[18] J. Pauly, D. Nishimura, A. Macovski, A linear class of large tip-angle selective excitation pulses, J. Magn. Res. 82 (1989) 571–587.
[19] S. Meiboom, D. Gill, Modified spin-echo method for measuring nuclear relaxation times, Rev. Sci. Instrum. 29 (1958) 688–691.
[20] J. Pauly, P. Le Roux, D. Nishimura, A. Macovski, Parameter relations for the Shinnar-Le Roux selective excitation pulse design algorithm, IEEE Trans. Med. Imag. 10 (1) (1991) 53–65.
[21] Y. Zur, M.L. Wood, L.J. Neuringer, Motion insensitive steady-state free precession imaging, Magn. Reson. Med. 16 (1990) 444–459.
[22] D.I. Hoult, R.E. Richards, The signal to noise ratio of the nuclear magnetic resonance experiment, J. Magn. Res. 24 (1976) 71–85.
[23] A. Blank, G. Alexandrowicz, L. Muchnik, G. Tidhar, R. Virmani, J. Schneiderman, E. Golan, Miniature self-contained NMR probe for clinical applications, J. Magn. Reson. (submitted).
[24] R.N. Bracewell, The Fourier Transform and its Applications, McGraw-Hill, New York, 1986 (Chapter 18, p. 362).
[25] D.G. Norris, P. Bornert, T. Reese, D. Liebfritz, On the application of Ultra-fast RARE experiments, Mag. Res. Med. 27 (1992) 142–164.
[26] F. Schick, SPLICE: sub-second diffusion-sensitive MR imaging using a modified Fast Spin-Echo acquisition mode, Mag. Res. Med. 38 (1997) 638–644.
[27] Y.Q. Song, M.D. Hurlimann, C. Flaum, A method for rapid characterization of diffusion, J. Magn. Res. 161 (2003) 222–233.
[28] A. Abragam, The Principles of Nuclear magnetism, Oxford University Press, New York, 1961 (Chapter 3).